AMC2014-Yokohama
March 14-16, 2014, Yokohama, Japan

Visual Feedback Control Method of a Wheeled Mobile Robot Using a Pan Camera Preferentially

Takafumi Ebata
Seikei University
Tokyo, Japan

Masahide Ito
Aichi Prefectural University
Aichi, Japan

Masaaki Shibata
Seikei University
Tokyo, Japan

***Abstract*—This paper addresses a vision-based control problem for a wheeled mobile robot with a pan camera (WMR+PC). The control inputs of the WMR+PC consist of pan rotational velocity of the camera and linear and angular velocities of the platform. When we adopt all three inputs for image-based visual servoing (IBVS), the standard IBVS controller dose not work at all due to the singularity of a Jacobian matrix which depends on the configuration of the pan camera. For avoiding the singularity, we propose a new visual feedback control method using a pan camera preferentially without switching. The effectiveness of the proposed method demonstrates experimentally, in particular, for case that a target object moves transversaly.**

I. Introduction

Robotic systems need the ability to understand their workspace to behave autonomously. For this purpose, a camera is a very useful sensory device to provide a vision function for robots. An image captured via the camera contains a vast amount of information of the workspace. Introducing visual information extracted from an image into a robot control loop has the potential to increase the flexibility and accuracy of a given task. In particular, feedback control with visual information, so-called *visual servoing* or *visual feedback control*, is a considerable technique for robot systems.

Visual servoing is classified into two basic approaches: position-based visual servoing (PBVS) and image-based visual servoing (IBVS). The difference between the PBVS and IBVS approaches depends on how to use visual feature of a target object which are extracted from image. One advantage of IBVS approach over the PBVS approach is robustness against modeling errors and external disturbances.

The IBVS controller is well-implemented for various robotic systems in the eye-in-hand configuration. A wheeled mobile robot (WMR) is often used for eye-in-hand configuration. The simplest system structure is consisted of fixed camera and platform with two independent motorized wheels. However, due to kinematic nonholonomic constraints, it is difficult to achieve an IBVS task. One way to reduce the affect is to interchange the fixed camera with the active camera.

A vision-based control problem for nonholonomic WMR with a pan camera (WMR+PC) is discussed in some literature [1]–[4]. E. Low, *et al.* [1] presents a biologically-inspired controller with the optical flow and geometrical consideration achieve positioning a WMR to a target object at a certain location heading. Y. Fang, *et al.* [2] presents an active visual servoing strategy combined with an adaptive vision tracking controller for the camera and switched controller for platform configuration. S. Komada, *et al.* [3] was proposed a vision-based navigation method which consists of two parts: one is an IBVS controller for the pan angle of the camera and the other is velocity controller with geometrical information for the position and orientation of the platform. A vision-based control problem for WMR+PC is discussed the control inputs of the WMR+PC consist of a pan rotational velocity of the camera and linear and angular velocities of the platform. In [4], we pointed out that the standard IBVS controller dose not work at all due to the singularity of a Jacobian matrix. For avoiding the singularity, we also proposed a switching control strategy which consists of two modes: One is for IBVS using two control inputs, and the other is for regulating the platform orientation. However, switching is not desired from the impractical and energy-consuming point-of-view.

In this paper, we present a visual feedback control method of WMR using a pan camera preferentially. The difference between the previous work [4] and the proposed method is smoothness in the controller. The former is with switching, but the latter is without switching. Based on the experimental results for two cases, We discuss the performance of the proposed method.

II. Model of a Wheeled Mobile Robot with a Pan Camera

This section provides the vision and the robot models of a WMR+PC. Two kind of Jacobian matrices given from these models play important role in IBVS. In this paper, the target object is assumed to be static.

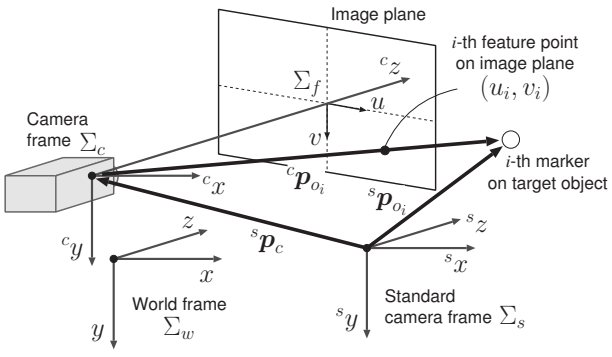

Fig. 1. Vision system model

A. Vision System Model

A target object is equipped with k markers. We refer to the markers as feature points on the image plane. The geometric relation between the camera and the i-th marker is depicted in Fig. 1, where the coordinate frames Σ_w, Σ_c, Σ_s, and Σ_f represent the world frame, the camera frame, the standard camera frame, and image plane frame, respectively. The frame Σ_s is static on Σ_w at a given time, which measures the velocity of Σ_c. The frame Σ_f is located at the center of image plane. Let ${}^s\boldsymbol{p}_{o_i} \in \mathbb{R}^3$, ${}^s\boldsymbol{p}_c \in \mathbb{R}^3$, and ${}^c\boldsymbol{p}_{o_i} := [{}^cx_{o_i}, {}^cy_{o_i}, {}^cz_{o_i}]^\top$ be the position vectors of the i-th marker on Σ_s, the camera on Σ_s, and the i-th marker on Σ_c, respectively. The coordinates of the i-th feature point on Σ_f are denoted as $\boldsymbol{f}_i = [u_i, v_i]^\top$.

When the camera moves at a certain translational and angular velocity for a stationary target object on Σ_s (i.e.,${}^s\boldsymbol{p}_{o_i} \equiv \boldsymbol{0}_3$), the translational velocity of the i-th marker on Σ_c can be represented as

$$ {}^c\dot{\boldsymbol{p}}_{o_i} = -{}^s\dot{\boldsymbol{p}}_c - {}^s\boldsymbol{\omega}_c \times {}^c\boldsymbol{p}_{o_i}, \tag{1} $$

where ${}^s\boldsymbol{\omega}_c$ is the angular velocity of the camera on Σ_s. We assume an ideal pinhole camera model as an imaging model. Then, from the perspective projection, the i-th feature point can be expressed as

$$ \boldsymbol{f}_i = \begin{bmatrix} u_i \\ v_i \end{bmatrix} := \frac{1}{{}^cz_{o_i}} \begin{bmatrix} \lambda_x {}^cx_{o_i} \\ \lambda_y {}^cy_{o_i} \end{bmatrix}, \tag{2} $$

where λ_x and λ_y are the horizontal and vertical focal lengths of the camera, respectively. By using (1) and differentiating (2) with respect to time, we obtain

$$ \dot{\boldsymbol{f}}_i := \boldsymbol{J}_{\text{img}}(\boldsymbol{f}_i, {}^cz_{o_i}) {}^s\boldsymbol{w}_c. \tag{3} $$

where $\boldsymbol{J}_{\text{img}} = \begin{bmatrix} \boldsymbol{J}_{\text{img}}^{(1,1)} & \boldsymbol{J}_{\text{img}}^{(1,2)} \end{bmatrix} \in \mathbb{R}^{2\times 6}$,

$$ \boldsymbol{J}_{\text{img}}^{(1,1)}(\boldsymbol{f}_i, {}^cz_{o_i}) := \begin{bmatrix} -\frac{\lambda_x}{{}^cz_{o_i}} & 0 & \frac{u_i}{{}^cz_{o_i}} \\ 0 & -\frac{\lambda_y}{{}^cz_{o_i}} & \frac{v_i}{{}^cz_{o_i}} \end{bmatrix}, $$

$$ \boldsymbol{J}_{\text{img}}^{(1,2)}(\boldsymbol{f}_i) := \begin{bmatrix} \frac{1}{\lambda_y}u_iv_i & -\left(\lambda_x + \frac{u_i^2}{\lambda_x}\right) & \frac{\lambda_x}{\lambda_y}v_i \\ \lambda_y + \frac{v_i^2}{\lambda_y} & -\frac{1}{\lambda_x}u_iv_i & -\frac{\lambda_y}{\lambda_x}u_i \end{bmatrix}, $$

and ${}^s\boldsymbol{w}_c = [{}^s\dot{\boldsymbol{p}}_c^\top, {}^s\boldsymbol{\omega}_c^\top]^\top \in \mathbb{R}^6$ is called the velocity twist of the camera. Summarizing (3) in term of k feature points, we obtain

$$ \dot{\boldsymbol{f}} = \bar{\boldsymbol{J}}_{\text{img}}(\boldsymbol{f}, {}^c\boldsymbol{z}_o) {}^s\boldsymbol{w}_c, \tag{4} $$

where $\boldsymbol{f} := [\boldsymbol{f}_1^\top, \cdot, \boldsymbol{f}_k^\top]^\top \in \mathbb{R}^{2k}$, ${}^c\boldsymbol{z}_o = [{}^cz_{o_1}, \cdot, {}^cz_{o,k}]^\top \in \mathbb{R}^k$, $\bar{\boldsymbol{J}}_{\text{img}} := [\boldsymbol{J}_{\text{img}}^\top(\boldsymbol{f}_1, {}^cz_{o_1}), \cdot, \boldsymbol{J}_{\text{img}}^\top(\boldsymbol{f}_1, {}^cz_{o_k})]^\top \in \mathbb{R}^{2k\times 6}$. The matrix $\bar{\boldsymbol{J}}_{\text{img}}$ is the so-called *image Jacobian matrix*.

B. Robot system Model

The model of the WMR+PC is depicted in Fig. 2. The right and left wheeled and the camera, which are actuated independently, are provided at the front of the robot. A passively revolving caster is also provided at rear of the robot. The coordinate frames Σ_w and Σ_c are the same world and camera frames as in Fig. 1. The vehicle body frame Σ_b is located at the bottom of the perpendicular line from the barycenter of the vehicle body to the axle. Note that y- and ${}^by$-axes are not considered in modeling in this section. the parameters are defined as in Table I. Assuming that each wheel dose not skid or slip on the ground, the origin of Σ_b can move only along the ${}^bz$-axis instantaneously. This can be described by the formula $\dot{x} = \nu_1 \cos\theta$ and $\dot{z} = \nu_1 \sin\theta$, or the equivalent expression

$$ \dot{x} = \dot{z}\tan\theta \quad \Leftrightarrow \quad \dot{x}\cos\theta - \dot{z}\sin\theta = 0. \tag{5} $$

Equation (5) is non-integrable differential equation which is described by the position, a so-called *non-holonomic constraint* [5].

The velocity twist of the camera ${}^s\boldsymbol{w}_c$ is associated with the input $\boldsymbol{\nu}$ as follows [4]:

$$ {}^s\boldsymbol{w}_c = \underbrace{\begin{bmatrix} -\sin\phi_c & {}^bx_c\sin\phi_c + {}^bz_c\cos\phi_c & 0 \\ 0 & 0 & 0 \\ \cos\phi_c & -{}^bx_c\cos\phi_c + {}^bz_c\sin\phi_c & 0 \\ 0 & 0 & 0 \\ 0 & 1 & 1 \\ 0 & 0 & 0 \end{bmatrix}}_{{}^c\boldsymbol{J}(\phi_c)} \boldsymbol{\nu}, \tag{6} $$

where $\boldsymbol{\nu} = [\nu_1, \nu_2, \nu_3]^\top$. Also, the geometric relation between $\boldsymbol{\nu}$

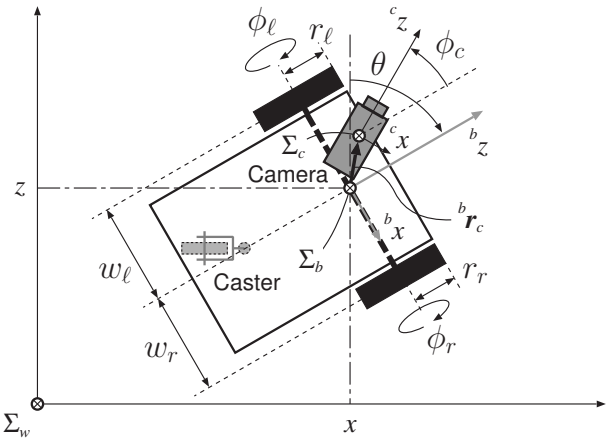

Fig. 2. Robot system model with single camera

TABLE I
PARAMETERS OF THE ROBOT

(x, z)	: origin coordinates of Σ_b on Σ_w
θ	: angle of the traveling direction w.r.t the z-axis (i.e positive direction of the ${}^bz$-axis w.r.t the z-axis)
ϕ_r, ϕ_ℓ	: rotating angles of the right and left wheels
ϕ_c	: pan rotating angle of the camera w.r.t the ${}^bz$-axis ($\boldsymbol{\phi} := [\phi_r, \phi_\ell, \phi_c]^\top$)
w_r, w_ℓ	: distance between the origin of Σ_b and the right/left wheel
${}^b\boldsymbol{r}_c$	: position vector of Σ_c on Σ_b (${}^b\boldsymbol{r}_c := [{}^bx_c, {}^bz_c]^\top$)
r_r, r_ℓ	: radii of the right and left wheels
ν_1	: longitudinal velocity of the platform in Σ_b
ν_2	: angular velocity of the platform around the ${}^by$-axis
ν_3	: angular velocity of the camera around the ${}^cy$-axis
m	: mass of the car
r	: radius of the wheel
w	: length of shaft
J_n	: inertia of the car
I_n	: inertia of the wheel

and $\dot{\boldsymbol{\phi}} := [\dot{\phi}_r, \dot{\phi}_\ell, \dot{\phi}_c]^\top$ is expressed as:

$$\boldsymbol{\nu} = \underbrace{\begin{bmatrix} \frac{w_\ell r_r}{w_r+w_\ell} & \frac{w_r r_\ell}{w_r+w_\ell} & 0 \\ \frac{r_r}{w_r+w_\ell} & -\frac{r_\ell}{w_r+w_\ell} & 0 \\ 0 & 0 & 1 \end{bmatrix}}_{\boldsymbol{T}_w} \dot{\boldsymbol{\phi}}. \tag{7}$$

Note that the column rank of the ${}^c\boldsymbol{J}(\phi_c)$ depends on the value of ${}^b\boldsymbol{z}_c$, i.e., the camera configuration on the platform. The fact is derived from the following determinant of the *robot Jacobian matrix* ${}^c\boldsymbol{J}(\phi_c)$:

$$\det {}^c\boldsymbol{J}^\top {}^c\boldsymbol{J} = {}^bx_c^2 + {}^bz_c^2 + 1 - (-{}^bx_c)^2 - 1 = {}^bz_c^2.$$

If ${}^bz_c \neq 0$, then rank ${}^c\boldsymbol{J}(\phi_c) = 3\ \forall\phi_c$, i.e., ${}^c\boldsymbol{J}$ is full column rank; If ${}^bz_c = 0$, then rank ${}^c\boldsymbol{J}(\phi_c) = 2\ \forall\phi_c$. The former case means that we cannot design a standard IBVS controller using the pseudo-inverse of the composite matrix $\bar{\boldsymbol{J}}_{\rm img}{}^c\boldsymbol{J}$ (or $\bar{\boldsymbol{J}}_{\rm img}{}^c\boldsymbol{J}\boldsymbol{T}_w$) when the camera is located along the ${}^bx$-axis. A similar argument is also in [4]. For avoiding the singularity, the authors proposed a switching control strategy which consists of two modes [4]. However, due to switching, this strategy is inefficient in energy from a practical point-of-view. To overcome this drawback, we present a new visual feedback control method without switching in the next section.

III. Visual Feedback Control Method

This section presents visual feedback control method for case that the camera is located along the ${}^bx$-axis. In that case, ${}^c\boldsymbol{J}$ is described as

$${}^c\boldsymbol{J}(\phi_c) = \begin{bmatrix} -\sin\phi_c & {}^bz_c\cos\phi_c & 0 \\ 0 & 0 & 0 \\ \cos\phi_c & {}^bz_c\sin\phi_c & 0 \\ 0 & 0 & 0 \\ 0 & 1 & 1 \\ 0 & 0 & 0 \end{bmatrix},$$

In a manner similar to [4], as submatrices of ${}^c\boldsymbol{J}$, two Jacobian matrices are defined as

$${}^c\boldsymbol{J}_{12}(\phi_c) = \begin{bmatrix} -\sin\phi_c & {}^bz_c\cos\phi_c \\ 0 & 0 \\ \cos\phi_c & {}^bz_c\sin\phi_c \\ 0 & 0 \\ 0 & 1 \\ 0 & 0 \end{bmatrix} \quad \text{for} \quad \boldsymbol{\nu}_{12} := [\nu_1, \nu_2]^\top, \tag{8}$$

and

$${}^c\boldsymbol{J}_{13}(\phi_c) = \begin{bmatrix} -\sin\phi_c & 0 \\ 0 & 0 \\ \cos\phi_c & \\ 0 & 0 \\ 0 & 1 \\ 0 & 0 \end{bmatrix} \quad \text{for} \quad \boldsymbol{\nu}_{13} := [\nu_1, \nu_3]^\top. \tag{9}$$

Both matrices are full column rank without depending on values of ${}^bz_c$ and ϕ_c. Furthermore, if ${}^bz_c = 0$, then ${}^c\boldsymbol{J}_{12} = {}^c\boldsymbol{J}_{13}$.

Limiting the original control input $\boldsymbol{\nu}$ to $\boldsymbol{\nu_{12}}$ or $\boldsymbol{\nu_{13}}$, we can design the IBVS control system. Now we select $\boldsymbol{\nu}_{13}$ for IBVS using a pan camera preferentially.

From (3) and (9), $\dot{\boldsymbol{f}}$ is associated with $\boldsymbol{\nu_{13}}$ as follows:

$$\dot{\boldsymbol{f}} = \boldsymbol{J}_{\rm vis}(\boldsymbol{f}, {}^cz_o, \phi_c)\boldsymbol{\nu}_{13}. \tag{10}$$

where $\boldsymbol{J}_{\rm vis} = \bar{\boldsymbol{J}}_{\rm img}{}^c\boldsymbol{J}_{13}(\phi_c) \in \mathbb{R}^{2k\times 2}$. Considering a minimization problem

$$\min_{\boldsymbol{\nu}_{13}} \|\dot{\boldsymbol{f}} - \boldsymbol{J}_{\rm vis}(\boldsymbol{f}, {}^cz_o, \phi_c)\boldsymbol{\nu}_{13}\|,$$

a solution under the condition rank $\boldsymbol{J}_{\rm vis} = 2$ is

$$\boldsymbol{\nu}_{13} = \boldsymbol{J}_{\rm vis}^+(\boldsymbol{f}, {}^cz_o, \phi_c)\dot{\boldsymbol{f}}, \tag{11}$$

where $\boldsymbol{J}_{\rm vis}^+$ denotes the pseudo-inverse of $\boldsymbol{J}_{\rm vis}$. The matrix $\boldsymbol{J}_{\rm vis}^+$ is described as

$$\boldsymbol{J}_{\rm vis}^+ = \begin{cases} \boldsymbol{J}_{\rm vis}^{-1}, & \text{for } k = 1 \\ (\boldsymbol{J}_{\rm vis}\boldsymbol{J}_{\rm vis}^T)^{-1}\boldsymbol{J}_{\rm vis}^T, & \text{for } k > 1 \end{cases}$$

Note that rank $\boldsymbol{J}_{\rm vis} = 2$ always holds for all ϕ_c, which implies that $\boldsymbol{J}_{\rm vis}$ is non-singular without depending on the number of feature points.

The control objective is to make each feature point $\boldsymbol{f}_i$ converge into the desired one $\boldsymbol{f}_i^d (i = 1, \ldots, k)$. To achieve this objective for the feature point dynamics

$$\dot{\boldsymbol{f}} = \boldsymbol{\mu}, \tag{12}$$

where $\boldsymbol{\mu}$ denotes the linear control input on Σ_f, we adopt the proportional controller

$$\boldsymbol{\mu} = \boldsymbol{K}_{\rm img}(\boldsymbol{f}^d - \boldsymbol{f}). \tag{13}$$

where $\boldsymbol{K}_{\rm img} = \text{block diag}\ (\boldsymbol{K}_{\rm img1}, \ldots, \boldsymbol{K}_{\rm imgk}) \in \mathbb{R}^{2k\times 2k}$, $\boldsymbol{K}_{\rm imgi} := \text{diag}\ (K_{\rm img1i}^u, K_{\rm img1i}^v) \in \mathbb{R}^{2\times 2}$, $\boldsymbol{f}^d = [u_1^d, v_1^d, \ldots, u_k^d, v_k^d]^\top \in \mathbb{R}^{2k}$. From (11), (12) and (13), the control input $\boldsymbol{\nu}_{13}$ is therefore given by

$$\boldsymbol{\nu}_{13} = \boldsymbol{J}_{\rm vis}^+(\boldsymbol{f}, {}^cz_o, \phi_c)\boldsymbol{K}_{\rm img}(\boldsymbol{f}^d - \boldsymbol{f}). \tag{14}$$

On the other hand, the residual control input ν_2 is used for controlling the mobile platform orientation according to the pan rotation. We introduce a method that regulates the platform orientation so as to head the camera toward the forwarding direction of the platform. We design the following proportional feedback controller:

$$\nu_2 = K_o\{(\theta + \phi_c) - \theta\} = K_o\phi_c, \tag{15}$$

where $K_o > 0$ is proportional feedback gain. Equation (15) means that the angular velocity of the platform depends on angle of the pan camera. Consequently, we design a controller which follows the mobile platform orientation according to the pan camera smoothly. Using (14) and (15), our proposed feedback controller is synthesized. The angular velocity command $\dot{\boldsymbol{\phi}}^d = [\dot{\phi}_r^d, \dot{\phi}_\ell^d, \dot{\phi}_c^d]^\top$ is therefore given by

$$\dot{\boldsymbol{\phi}}^d = \boldsymbol{T}_w^{-1}\boldsymbol{\nu}. \tag{16}$$

The step-by-step integration of $\dot{\boldsymbol{\phi}}^d$ with respect to time can calculate the desired angle $\boldsymbol{\phi}^d$. In order to control each angle and angular velocity of the wheels and the ${}^cy$-axis, we here

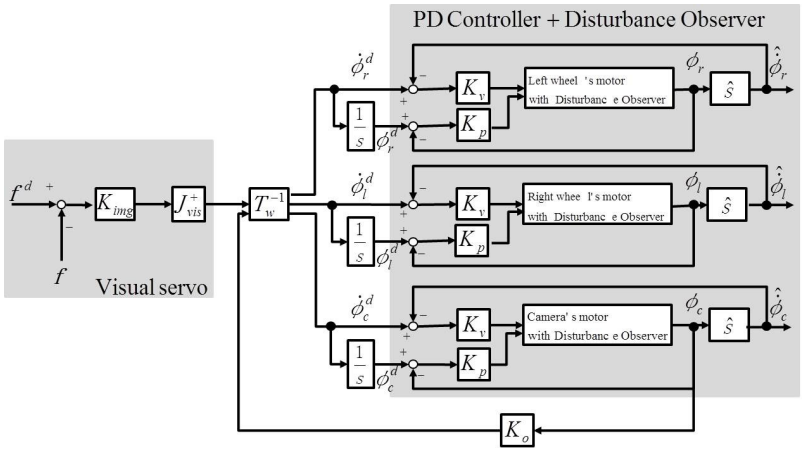

Fig. 3. Whole control system

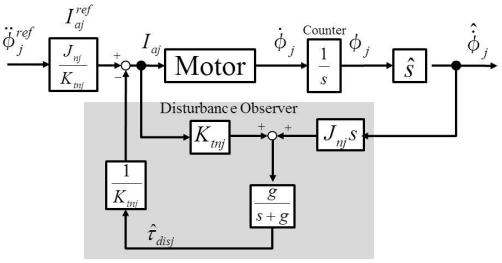

Fig. 4. Disturbance rejection using disturbance observer

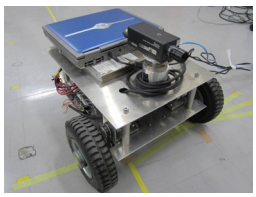

Fig. 5. WMR+PC

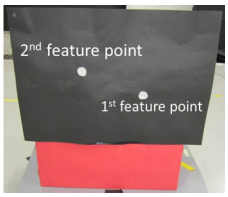

Fig. 6. Target object

adopt the following PD feedback control with disturbance rejection based on the disturbance observer [6].

$$\ddot{\phi}_j^{ref} = K_p(\phi_j^d - \phi_j) + K_v(\dot{\phi}_j^d - \dot{\phi}_j). \quad (j = r, \ell, c) \tag{17}$$

By using this controller with well-tuned design parameters, the angle and angular velocity can track the desired trajectories. The block diagram of the whole system is shown in Fig. 3. Disturbance generated at each motor in the whole control system is attenuated by using disturbance observer as shown in Fig. 4.

In the next section, we verify the effectiveness of our proposed method via experiments.

IV. Experiment

This section presents experimental results to validate the effectiveness of our proposed method. The control method is implemented for a WMR+PC, as depicted in Fig. 5. Here we consider the case where the number of markers is 2 (i.e., $k = 2$). Fig. 6 also shows the target object. For the sake of simplicity to detect the target object, makers are attached on the front of the target object.

A. Experimental Setup

The robot is equipped with two PCs, a CCD camera, three DC servo drivers, and three DC geared servo motors. One of the motor is used for panning the camera. The whole process was divided into two parts, each being handled by one of the PCs: one PC handles image processing and the other handles control.

The image resolution and the focal lengths of the CCD camera as 640×480 pixels and $\lambda_x(= \lambda_y) = 1090.3846$ pixels, respectively. The frame rate of the CCD camera was 60 fps. Hence, the image data was updated every 16.7 ms. In the image processing PC, image data obtained via the image capture board is binarized to extract the barycentric coordinates of each marker's area as the coordinates of each feature point. The

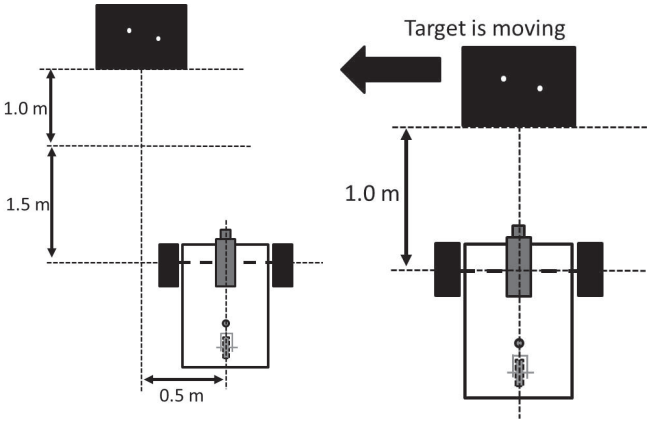

Fig. 7. Initial configuration in Experiment (i)

Fig. 8. Initial configuration in Experiment (ii)

coordinates of feature points were sent to the control PC via socket networking.

The PC for control runs a real-times Linux OS patched with real-time application interface (RTAI). The angle of rotation of each wheel was obtained from an encoder attached to each DC geared servo motor via a counter board. The coordinates of feature points are also received every 67 ms from the PC for image processing. Controlled armature current commands are sent to DC geared servo motors through DC servo drivers by a D/A converter. The control period is 1 ms.

Two kinds of experiments were performed. In Experiment (i), we verify that the proposed controller simultaneously achieve IBVS and regulating the platform orientation (pursuant to the pan camera angle). In Experiment (ii), we verify the effectiveness of our proposed method via comparing controller of WMR with fixed camera. Experiment (i) were performed under initial configuration depicted Fig. 7. In the case of experiment (i), the desired feature points and the depth were set to $\boldsymbol{f}_1^d = [77\,\text{pixels}, -3\,\text{pixels}]^\top$, $\boldsymbol{f}_2^d = [-72\,\text{pixels}, -6\,\text{pixels}]^\top$,

and ${}^{c}z_{c1} = 1.0(= {}^{c}z_{c2})$ m as constant values in the desired configuration. The main design parameters of the robot were as follows: $K_p = 400$, $\boldsymbol{K}_v = 40$, $\boldsymbol{K}_o = 0.25$, and $K^u_{\mathrm{imgi}} = 0.25(= K^v_{\mathrm{imgi}})(i = 1, 2)$. The procedure of Experiment (ii) is as follows:

Step 1 : As the initial configuration, locate the robot and the target object so as to capture all feature points around their desired coordinates.

Step 2 : Start the visual target following for the static target object using the proposed control method.

Step 3 : Let the target object go manually almost along the x-axis about 0.2 m/s for 5 s.

In the case of experiment (ii), the desired feature points and the depth were set to $\boldsymbol{f}^d_1 = [80\,\text{pixels}, -14\,\text{pixels}]^\top$, $\boldsymbol{f}^d_2 = [-62\,\text{pixels}, -68\,\text{pixels}]^\top$, and ${}^{c}z_{c1} = 1.0(= {}^{c}z_{c2})$ m as constant values in the desired configuration. The main design parameters of the robot were as follows: $K_p = 400$, $\boldsymbol{K}_v = 40$, $\boldsymbol{K}_o = 0.5$, and $K^u_{\mathrm{imgi}} = 0.25(= K^v_{\mathrm{imgi}})(i = 1, 2)$. For comparison, we consider a standard IBVS controller of WMR with fixed camera (WMR+FC). From (3), (7) and (8), $\dot{\boldsymbol{f}}$ is associated with $[\dot{\phi}_r, \dot{\phi}_\ell]^\top$ as follows:

$$\dot{\boldsymbol{f}} = \underbrace{\bar{\boldsymbol{J}}_{\mathrm{img}}(\boldsymbol{f}, {}^{c}z_o){}^{c}\boldsymbol{J}_{12}\begin{bmatrix} \frac{w_\ell r_r}{w_r+w_\ell} & \frac{w_r r_\ell}{w_r+w_\ell} \\ \frac{r_r}{w_r+w_\ell} & -\frac{r_\ell}{w_r+w_\ell} \end{bmatrix}}_{{}^{f}\boldsymbol{J}_{\mathrm{vis}}(\boldsymbol{f}, {}^{c}z_o)} \begin{bmatrix} \dot{\phi}_r \\ \dot{\phi}_\ell \end{bmatrix}. \tag{18}$$

Similarly to (14), we therefore design the desired trajectory of the angular velocity as follows:

$$\begin{bmatrix} \dot{\phi}^d_r \\ \dot{\phi}^d_\ell \end{bmatrix} = {}^{f}\boldsymbol{J}^{+}_{\mathrm{vis}}(\boldsymbol{f}, {}^{c}z_o)\boldsymbol{K}_{\mathrm{img}}(\boldsymbol{f}^d - \boldsymbol{f}). \tag{19}$$

The step-by-step integration of $\dot{\boldsymbol{\phi}}^d$ with respect to time can calculate the desired angle $\boldsymbol{\phi}^d$.

B. Results and Discussion

Fig. 9 shows results of Experiment (i). Figs.10 and 11 also show results Experiment (ii).

From Fig. 9, $\boldsymbol{f}$ converged into admissible neighborhood of $\boldsymbol{f}^d$. The convergence time was long. The reason is that the value of $\boldsymbol{K}_{\mathrm{img}}$ were set to small. The platform orientation was regulated so as to converge the pan camera angle into zero. Consequently, the camera was headed toward the forwarding direction of platform.

From Fig. 10, the error $\boldsymbol{f}^d - \boldsymbol{f}$ enlarged gradually in the conventional method. On the other hand, from Fig. 11, the error $\boldsymbol{f}^d - \boldsymbol{f}$ was converged to zero gradually after it enlarged temporariy. Therefore, the proposed controller for WMR+PC is more effective than the standard IBVS controller for WMR+FC in the visual feedback control for the target object moving transversely. Also, from Figs.10 (c) and 11 (c), we found that angular velocity needed by the proposed controller is relatively small. However, it is difficult for the proposed controller to converge the error $\boldsymbol{f}^d - \boldsymbol{f}$ into zero completely. For this difficulty, the authors consider that the proposed controller furthermore needs compensation of the motion of the target object.

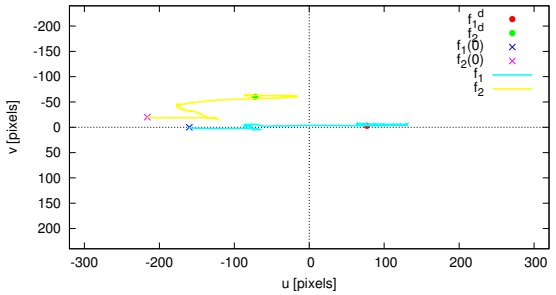

(a) Trajectories of two feature points on the image plane

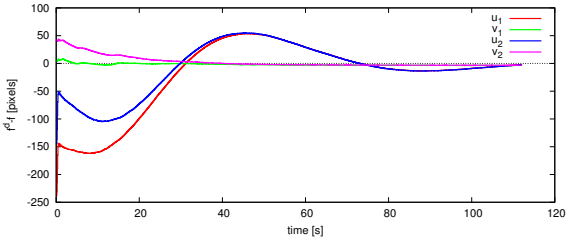

(b) Time response of $\boldsymbol{f}^d - \boldsymbol{f}$

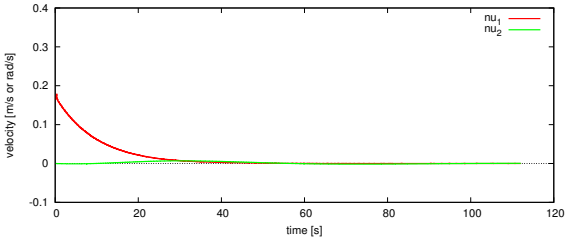

(c) Time response of $\boldsymbol{\nu}$

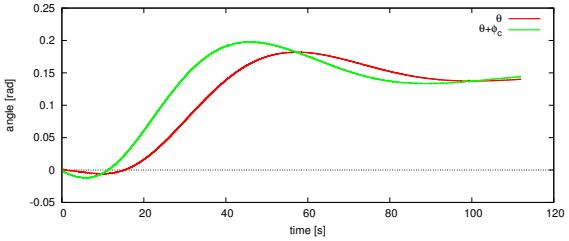

(d) Time response of ϕ_c

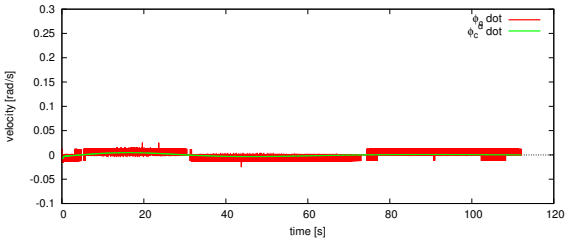

(e) Time response of $\dot{\phi}_c$

Fig. 9. Results of Experimental (i)

V. Conclusions

We have proposed a visual feedback control method for a WMR using a pan camera preferentially. In consideration of structure of the robot matrix, an proposed controller using the platform's linear velocity and camera's pan angular velocity

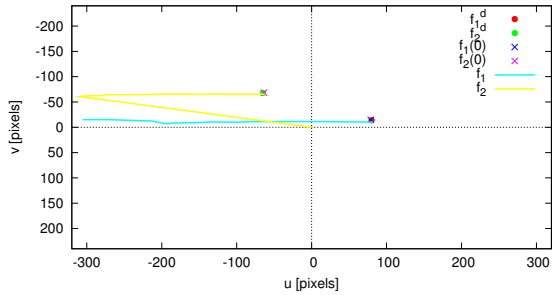

(a) Trajectories of two feature points on the image plane

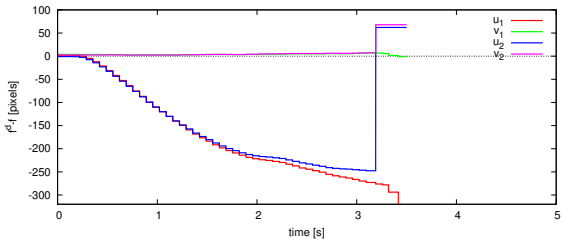

(b) Time response of $\boldsymbol{f}^d - \boldsymbol{f}$

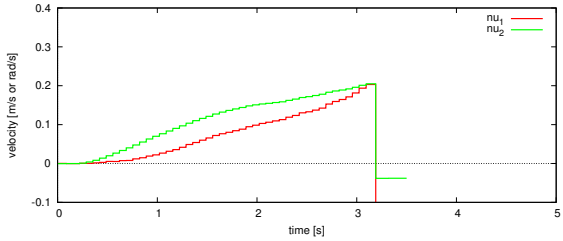

(c) Time response of $\boldsymbol{\nu}$

Fig. 10. Results of Experimental (ii) in the case of using a standard IBVS controller for WMR+FC

for IBVS while exploits the angular velocity of the platform for controlling the mobile platform orientation according to the pan rotation. We have verified the effectiveness of our proposed method via two experiments.

In future work, we will consider the motion estimation of the target object.

References

[1] E. M. P. Low, I. R. Manchester, and A. V. Savkin: "A biologically inspired method for vision-based docking of wheeled mobile robots," *Robotics and Autonomous Systems*, Vol. 55, pp. 769–784, 2007.

[2] Y. Fang, X. Liu, and X. Zhang: "adoptive active visual servoing of nonholonomic mobile robots," IEEE Trans. Ind. Electron. Vol. 59, No. 1, pp. 486–497, 2012.

[3] S. Komada, K. Kinosita, T. Hirukawa, and J. Hirai: "Image feature based navigation of nonholonomic mobile robot with active camera," In *Proc. of the 17th IFAC World Congress (IFAC'08)*, pp. 14714–14719, 2008.

[4] M. Ito, T. Ebata, and M. Shibata: "Vision-based switching control strategy for a nonholonomic wheeled mobile robot with a pan camera," *Proc. of 9th International Workshop on Robot Motion Control*, pp. 30–35, 2013.

[5] R. W. Brockett: "Asymptotic stability and feedback stabilization," *Differential Geometric Control Theory*, pp. 181–192, 1983.

[6] K. Ohnishi, M. Shibata, and T. Murakami: "Motion control for advanced mechatronics," *IEEE/ASME Trans. Mechatronics*, Vol. 1, pp. 56–67, 1996.

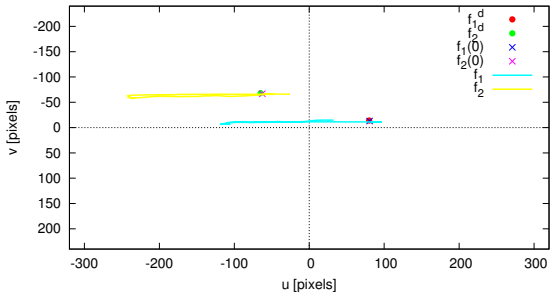

(a) Trajectories of two feature points on the image plane

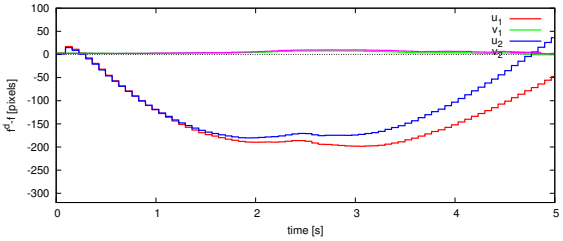

(b) Time response of $\boldsymbol{f}^d - \boldsymbol{f}$

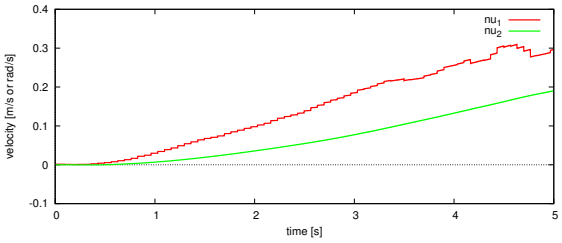

(c) Time response of $\boldsymbol{\nu}$

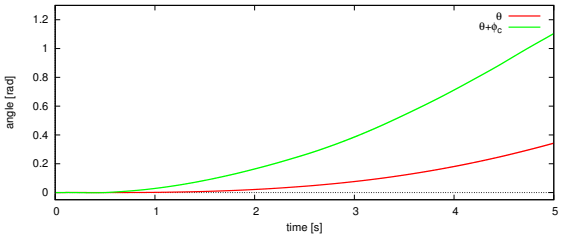

(d) Time response of ϕ_c

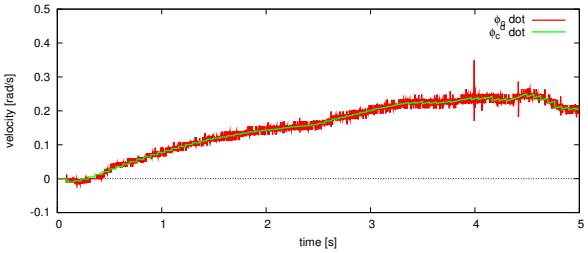

(e) Time response of $\dot{\phi}_c$

Fig. 11. Results of Experimental (ii) in the case of using the proposed controller for WMR+PC